Effect of Daily Temperature Fluctuations on Virus Lifetime

Te Faye Yap, [1] Colter J. Decker, [1] Daniel J. Preston[1,*]

[1]Department of Mechanical Engineering, Rice University, 6100 Main St., Houston, TX 77005

*Corresponding author: djp@rice.edu

DOI: https://doi.org/10.1016/j.scitotenv.2021.148004

Highlights

- Daily temperature fluctuations are inversely correlated with virus lifetimes.
- This work provides a physical explanation for the observed correlation.
- Chemical kinetics describes the temperature-dependent rate of virus inactivation.
- Higher daily temperature range (DTR) results in shorter virus lifetimes.
- The effects of daily mean temperature and DTR are shown for SARS-CoV-2.

Abstract

Epidemiological studies based on statistical methods indicate inverse correlations between virus lifetime and both (i) daily mean temperature and (ii) diurnal temperature range (DTR). While thermodynamic models have been used to predict the effect of constant-temperature surroundings on virus inactivation rate, the relationship between virus lifetime and DTR has not been explained using first principles. Here, we model the inactivation of viruses based on temperature-dependent chemical kinetics with a time-varying temperature profile to account for the daily mean temperature and DTR simultaneously. The exponential Arrhenius relationship governing the rate of virus inactivation causes fluctuations above the daily mean temperature during daytime to increase the instantaneous rate of inactivation by a much greater magnitude than the corresponding decrease in inactivation rate during nighttime. This asymmetric behavior results in shorter predicted virus lifetimes when considering DTR and consequently reveals a potential physical mechanism for the inverse correlation with DTR reported in statistical epidemiological studies. In light of the ongoing COVID-19 pandemic, a case study on the effect of daily mean temperature and DTR on the lifetime of SARS-CoV-2 was performed for the five most populous cities in the United States. In Los Angeles, where mean monthly temperature fluctuations are low (DTR ≈ 7 °C), accounting for DTR decreases predicted SARS-CoV-2 lifetimes by only 10%; conversely, accounting for DTR for a similar mean temperature but larger mean monthly temperature fluctuations in Phoenix (DTR ≈ 15 °C) decreases predicted lifetimes by 50%. The modeling framework presented here provides insight into the independent effects of mean temperature and DTR on virus lifetime, and a significant impact on transmission rate is expected, especially for viruses that pose a high risk of fomite-mediated transmission.

Keywords: Diurnal Temperature Range, Thermal Inactivation, Coronavirus, WAVE Model, SARS-CoV-2, COVID-19

Main Text

1. Introduction

Epidemiologists incorporate environmental effects when modeling the spread of diseases by applying statistical methods to determine whether environmental variables correlate with transmission rates (Malki et al., 2020; Rahman et al., 2020; Sajadi et al., 2020). Environmental temperature is often considered; however, most models only account for the daily mean temperature (Anver Sethwala, Mohamed Akbarally, Nathan Better, Jeffrey Lefkovits, Leeanne Grigg, 2020; Merow and Urban, 2020; Pirouz et al., 2020; Sajadi et al., 2020), despite studies reporting that the diurnal temperature range (DTR) also plays a significant role in forecasting the transmission of diseases (Islam et al., 2020; Liu et al., 2020; Luo et al., 2013; Ma et al., 2020; Merow and Urban, 2020). One recent study on the mosquito's (Aedes aegypti) ability to transmit dengue virus showed that an increase in DTR reduces transmission rates at mean temperatures above 18 °C (Lambrechts et al., 2011). This work studied the importance of considering both (i) daily mean temperatures and (ii) temperature fluctuations; the pathogen was transmitted by an active vector, where the virus lifetime may be less significant than in the case of a passive vector (e.g., fomite-mediated transmission), but DTR nevertheless played a role. Meanwhile, thermodynamic models built on first principles have been used to predict the lifetime of viruses based on constant-temperature surroundings (Yap et al., 2020), but a framework describing the relationship between virus inactivation rate and DTR has not been established.

The ongoing COVID-19 pandemic represents a critical area where such a fundamental physical model could find use. Recent literature describes epidemiological studies based on statistical analyses that document an inverse correlation between DTR and relative risk (RR), where RR represents the ratio of the probability of infection under a given condition to the probability of infection in a control group. For example, studies by Islam et al. and Liu et al. present statistical analyses accounting for DTR, and they both report a correlation coefficient between RR and DTR of less than one for COVID-19 (Islam et al., 2020; Liu et al., 2020), indicating lower

infection rates at higher values of DTR. A study conducted during the onset of the pandemic in China seemingly showed the opposite relationship, reporting a positive correlation of DTR with number of deaths due to COVID-19; however, higher DTR is also known to increase the overall risk of mortality (Kim et al., 2016), and as such, mortality can be a poor indicator for the rate of transmission in this context. More recent studies in India, Indonesia, and Russia report negative correlations between DTR and COVID-19 infection rates or number of cases (Pramanik et al., 2020; Pratim, 2020; Supari et al., 2020), which is likely attributable, at least in part, to shorter virus lifetimes outside of a host because fomites have served as a mode of transmission for other viruses (Abdelrahman et al., 2020; Boone and Gerba, 2007; Xiao et al., 2017). Although fomite-mediated transmission is not likely the primary mode of transmission for SARS-CoV-2, it still poses a risk (Bouchnita and Jebrane, 2020; Gao et al., 2021; Kampf et al., 2020; van Doremalen et al., 2020; Xiao et al., 2017; Zhao et al., 2020). These studies consider the aggregated statistical effects of environmental conditions to correlate DTR to number of cases, but they do not provide a fundamental understanding of the virus inactivation behavior.

Prior work introduced an analytical model that uses the rate law for a first-order reaction and the Arrhenius equation to predict the lifetime of coronaviruses as a function of constant temperature (Yap et al., 2020). This model treats viruses as macromolecules that are inactivated by thermal denaturation of the proteins comprising each virion to predict the time required to achieve an *n*-log inactivation, which is defined as the ratio of final viable concentration of a pathogen to its initial concentration in terms of 10 raised to the n^{th} power ($[C]/[C_0] = 10^{-n}$). For consistency throughout this work, we define the "lifetime" of a virus as the time required to achieve a 3-log reduction in concentration of that virus (i.e., $n = 3$) based on guidance from the US Food and Drug Administration (FDA); specifically, the FDA recommends a 3-log (99.9%) reduction in virus concentration for decontamination of non-enveloped viruses (CDC, 2008; FDA, 2020a, 2020b; Oral et al., 2020), which are typically more resistant to thermal inactivation than enveloped

77 viruses (Firquet et al., 2015; Yeo et al., 2020), allowing a conservative prediction of lifetime for
78 both types of viruses.

79 The lifetime of a virus has an exponential dependence on temperature, fundamentally
80 underpinning our hypothesis that accounting for environmental temperature fluctuations will
81 decrease virus lifetimes compared to relying only on daily mean temperature data. To further
82 explore this hypothesis, we introduced a numerical model to incorporate environmental
83 temperature fluctuations, enabling predictions of the lifetime of viruses and showing the disparities
84 between the computed virus lifetime when using (i) daily mean temperature only (i.e., a constant
85 daily temperature profile) and (ii) accounting for both daily mean temperature and DTR (i.e., a
86 time-varying temperature profile). **Figure 1** shows a graphical illustration of the difference
87 between models of virus lifetime based on these two profiles. The inactivation rate constant, k,
88 varies exponentially with temperature **(Figure 1(a))**, and this exponential dependence results in
89 temperature fluctuations above the mean influencing the instantaneous rate of inactivation to a
90 greater extent than fluctuations below the mean. **Figure 1(b)** shows the difference in inactivation
91 rate between the two temperature profiles. The plot on the right shows a greater increase in
92 magnitude of the instantaneous value of k as a result of temperature fluctuations above the daily
93 mean temperature (i.e., daytime) compared to the corresponding decrease in inactivation rate for
94 temperatures below the mean (i.e., nighttime), resulting in a shorter overall virus lifetime. The
95 illustration shows how incorporation of DTR generates shorter predicted virus lifetimes compared
96 to daily mean temperature alone. We also show that the virus lifetime will always decrease when
97 considering fluctuations in temperature in the Supplementary Material to provide a quantitative
98 fundamental understanding of the phenomenon. We compare the change in concentration at the
99 mean temperature to the change in concentration when considering temperature fluctuations

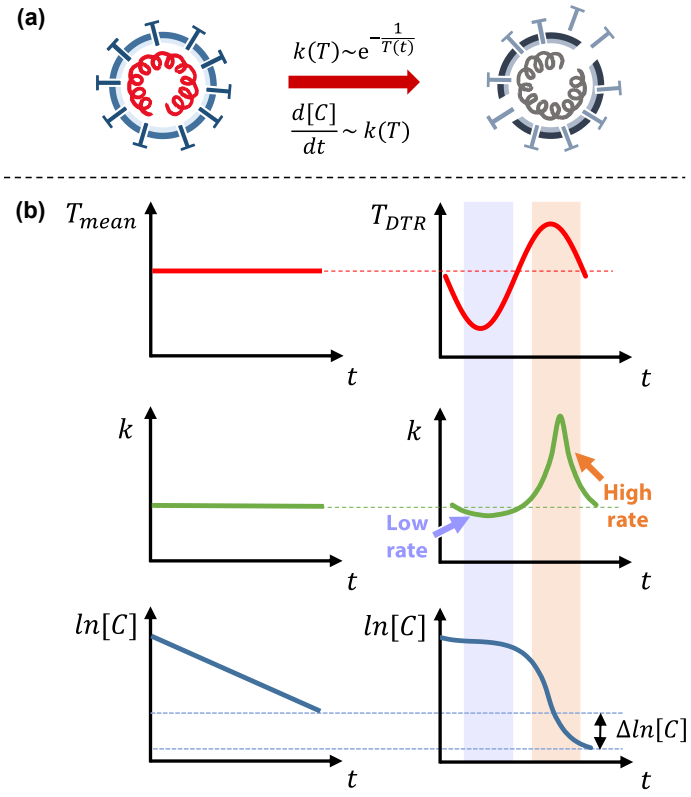

Figure 1 (Single Column). *The rate of inactivation of a virus depends on temperature following the rate law and Arrhenius equation (a). The effect of a time-varying temperature profile about the mean temperature influences the rate constant, k, for inactivation of a virus and, consequently, the concentration of a virus over time (b). The exponential dependence of the rate constant on temperature results in a higher net rate of inactivation of a virus when incorporating environmental temperature fluctuations about the mean temperature.*

while accounting for both symmetric and asymmetric time-varying temperature profiles. This physical behavior could explain the inverse correlation between DTR and RR observed in statistical epidemiological studies (Islam et al., 2020; Lambrechts et al., 2011; Lin et al., 2020; Liu et al., 2020; Pramanik et al., 2020; Pratim, 2020; Supari et al., 2020). We go on to present a case study on SARS-CoV-2 in the five most populous cities in the United States to illustrate the difference in virus lifetime when accounting for DTR. In this work, we model the inactivation rate

of viruses based on temperature-dependent chemical kinetics with a time-varying environmental temperature profile to account for the daily mean temperature and DTR simultaneously. This physical model of the effect of DTR on virus lifetime will elucidate the role of environmental temperature and the spread of viruses. We also show that this physical model can be applied to a range of coronaviruses, as well as influenza, which exhibits similar temperature-dependent inactivation behavior and seasonality (McDevitt et al., 2010). This work may provide an explanation as to why regions with similar daily mean temperatures may have starkly different virus transmission rates. Our model may also explain—at least in part—the surge of COVID-19 that has been observed in winter, as temperatures dropped and the virus lifetime increased by orders of magnitude.

2. Material and Methods

2.1 Theoretical Framework

The rate law for a first-order reaction (Eq. **1**) can be used to determine the inactivation of viruses (Yap et al., 2020).

$$\frac{d[C]}{dt} = -k(T) \cdot [C] \quad \textbf{[1]}$$

The rate constant, *k*, is governed by the Arrhenius equation, and can be determined for a given temperature. Previous models have considered only a constant temperature profile: temperature, *T,* did not vary with time, *t.* In this work, we calculate a time-varying rate constant as a function of a time-varying temperature profile using the Arrhenius equation (Eq. **2**):

$$k(T) = Ae^{-\frac{E_a}{RT(t)}} \quad \textbf{[2]}$$

where R is the gas constant, E_a is the activation energy associated with inactivation of the virus (i.e., the energy barrier that must be overcome for protein denaturation), and A is the frequency factor. The E_a and ln(A) values for SARS-CoV-2, SARS-CoV-1, and MERS-CoV were determined in prior work (Yap et al., 2020) and are reported in **Table 1**. The model can also be used to determine the lifetime of other viruses, including influenza viruses (responsible for the seasonal flu); we calculated values of E_a and ln(A) for Influenza A based on existing literature (McDevitt et al., 2010) to highlight the versatility of the model (primary data included in the Supplementary Material). These four enveloped viruses affect the respiratory system (Abdelrahman et al., 2020), and the corresponding results could be relevant to understanding the current pandemic (Abdelrahman et al., 2020; Zhu et al., 2020).

Environmental temperatures vary continuously with time, and this time-varying temperature profile can be used to determine the rate constant as a function of time. The daily temperature maximum, T_{max}, and minimum, T_{min}, are available for most regions with weather stations, while daily hourly temperature data are not often reported; therefore, we chose the WAVE diurnal temperature model introduced by de Wit, based on maximum and minimum temperature values, to represent the continuous daily temperature profile for a given location (Baker et al., 1988; Cesaraccio et al., 2001; Reicosky et al., 1989). Two half-cosine functions were used to estimate this diurnal temperature profile. For the first half-cosine function, the period, p_1, was calculated as the time between sunrise, when the minimum temperature occurs, and 1400 hours solar noon, when the maximum temperature occurs. The second half-cosine function continues from 1400 hours solar noon throughout the remainder of the 24-hour day for the second period, p_2, and joins with the first half-cosine function of the following day, d+1, at sunrise, where d represents the day for which the temperature used in the model is obtained. The sunrise times

in each city were obtained to determine the periods for the WAVE model. The temperature profile is defined by a piecewise function, given by Eq. **3**:

$$T(t) = \begin{cases} -\frac{T_{max,d}-T_{min,d}}{2} cos\left(\frac{\pi}{p_1}t\right) + \frac{T_{max,d}+T_{min,d}}{2}, & sunrise_d \le t < 1400\ hr_d \\ -\frac{T_{max,d}-T_{min,d+1}}{2} cos\left(\frac{\pi}{p_2}t - \frac{\pi}{p_2}p_1\right) + \frac{T_{max,d}+T_{min,d+1}}{2}, & 1400\ hr_d \le t < sunrise_{d+1} \end{cases} \quad \textbf{[3]}$$

The expression for the daily temperature profile (Eq. **3**) is substituted into Eq. **2**, which is then combined with Eq. **1**. Separation of variables is applied to yield the final expression used to determine the virus concentration after a given period of time:

$$\int_{[C]_0}^{[C]} \frac{d[C]}{[C]} = \int_{t_0}^{t} -A \exp\left(-\frac{E_a}{RT(t)}\right) dt \quad \textbf{[4]}$$

Due to the cumbersome temperature profile function, analytical integration of the right-hand side of Eq. **4** was not possible; we solved it numerically using Euler's method (details included in the Supplementary Material).

2.2 Data Collection

The daily sunrise times and maximum and minimum temperature data for the five cities with the highest populations in the United States were obtained from the National Oceanic and Atmospheric Administration (NOAA) solar calculator and climate data online search. A sinusoidal temperature profile that takes into account each city's maximum and minimum temperature was created for the period of January through December of 2020. The temperature profile, *T(t)*, was then used to solve for the reduction in concentration of virus as a function of time. The lifetime of the virus starting from sunrise on each calendar day was determined by calculating the concentration of viable virions as a function of the continuous temperature distribution over time, and then determining the time required to achieve a 3-log reduction in concentration. The

maximum cutoff point of the predicted lifetime was taken to be 30 days for two reasons: (i) to correspond approximately to one month, after which other the uncertainty in predictions becomes large due to other potential inactivation mechanisms (Yap et al., 2020); and (ii) to include the virus lifetime for the colder winter months through the end of November 2020 (the predicted virus lifetimes in some cities span more than one month, thus requiring temperature data from the subsequent month; at the time of preparing the results in this manuscript, only data through December 2020 were available). The n values were determined by taking the logarithm of the ratio of concentration at a given time, $[C]$, to the initial concentration, $[C]_0$.

2.3 Model Development: Activation Energy and Frequency Factor

The relevant physical parameters governing thermal inactivation of viruses were quantified from primary data reported in the literature. The log of concentration reported in primary experimental data on temperature-based inactivation of viruses, $\ln([C])$, was plotted as a function of time, t. According to the rate law for a first-order reaction (Eq. **1**), we determined the rate constant, k, for inactivation of a virus at a given temperature, T, by applying a linear regression and calculating the slope, $k = -\Delta\ln([C])/\Delta t$, as detailed in prior work (Yap et al., 2020). Each pair of k and T determined for a given virus was plotted; according to the Arrhenius equation (Eq. **2**), these data points yield a linear relationship between $\ln(k)$ and $1/T$. From the linear fit, the activation energy, E_a, and natural log of frequency factor, $\ln(A)$, can be obtained from the slopes and intercepts, respectively, of the fitted curves for each virus. These values were used in our analysis to determine the lifetimes of viruses in different regions as a function of daily mean temperature and daily temperature fluctuations using the numerical model presented in this work. The activation energy and frequency factor used here for SARS-CoV-2, SARS-CoV-1, and MERS-CoV were already determined in prior work (Yap et al., 2020), whereas the procedure used to determine the thermodynamic parameters used in this work for Influenza A is detailed in the Supplementary Material.

3. Results

The degree of inactivation of a virus, defined by the *n*-log reduction, is used to describe the order of magnitude decrease in virus concentration. The degree of inactivation is plotted against time to show the amount of time needed to achieve an *n*-log reduction, where **Figure 2** shows the lifetime (i.e., time until 3-log reduction) of three different coronaviruses and Influenza A computed using the time-varying temperature profile versus the daily mean temperature profile.

For illustration, temperature data for Houston starting on May 7 was used to determine the lifetime using the time-varying temperature profile versus the daily mean temperature profile. **Figure 2** shows the disparity in predicted lifetime when using the two different temperature profiles. In this case, when computing the lifetime of SARS-CoV-2 using daily mean temperatures **(Figure 2(a))**, it took approximately 3 days to achieve a 3-log reduction, whereas the more realistic time-varying environmental temperature profile **(Figure 2(b))** showed that decontamination would require less than 1.5 days. The reduction in predicted virus lifetime across all four viruses when accounting for the DTR was approximately 50%, highlighting the importance of DTR when modeling virus lifetime. All four of the viruses described in **Table 1** are modeled in **Figure 2**; however, due to the ongoing pandemic, only SARS-CoV-2 is emphasized throughout the remainder of this work.

For the top five most populous cities in the United States (New York City, Los Angeles, Chicago, Houston, and Phoenix), the lifetime of SARS-CoV-2 was calculated using the mean temperature profile and the time-varying temperature profile, with results plotted as blue and purple lines, respectively, in **Figure 3(a-e)**. The percentage difference in lifetime predictions for these two temperature profiles was also determined and plotted in red. The daily mean temperature and DTR values were averaged by month for each city and plotted in **Figure 3(f)** to show the monthly variation in temperature and provide a comparison between the cities. During the winter months with low daily mean temperatures, the virus lifetime can be greater than one

month; as the temperature increases during the summer, the lifetime of the virus becomes several orders of magnitude shorter. Cities like Los Angeles, which have relatively low variations

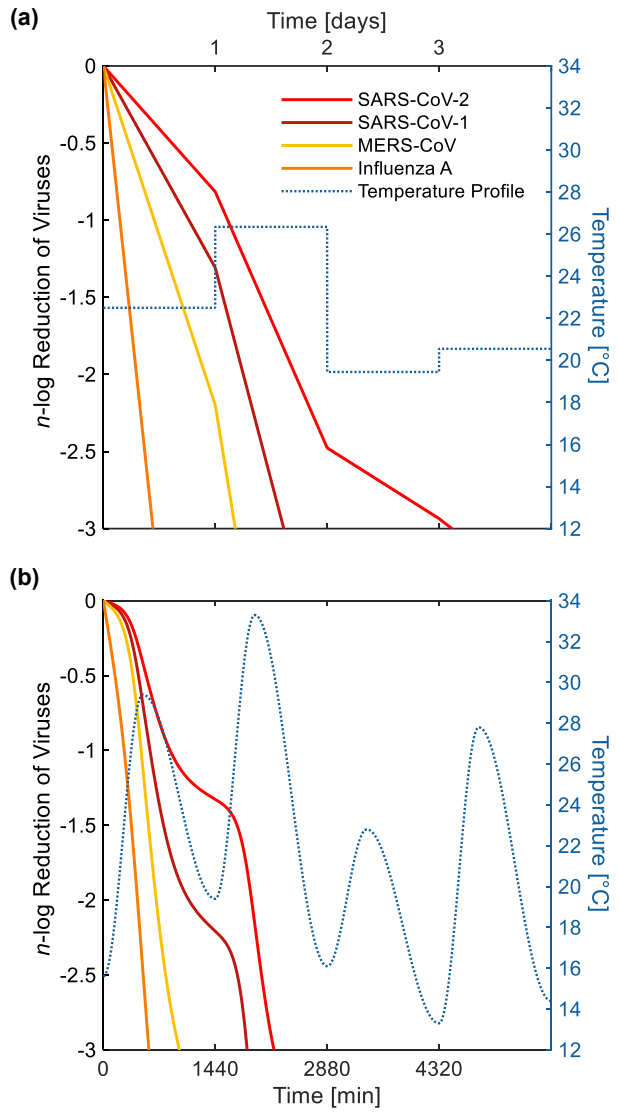

Figure 2 (Single Column). *Comparison of the degree of inactivation of three coronaviruses and Influenza A between (a) a simple daily mean temperature profile and (b) a time-varying temperature profile (temperature data shown for Houston starting on May 7). SARS-CoV-2 would require approximately 3 days to reach decontamination to a 3-log reduction in concentration according to the simple daily mean temperature model, whereas the more realistic time-varying environmental temperature profile showed that decontamination would require less than 1.5 days. The percentage difference in predicted lifetime across all four viruses when accounting for the DTR was approximately 50%.*

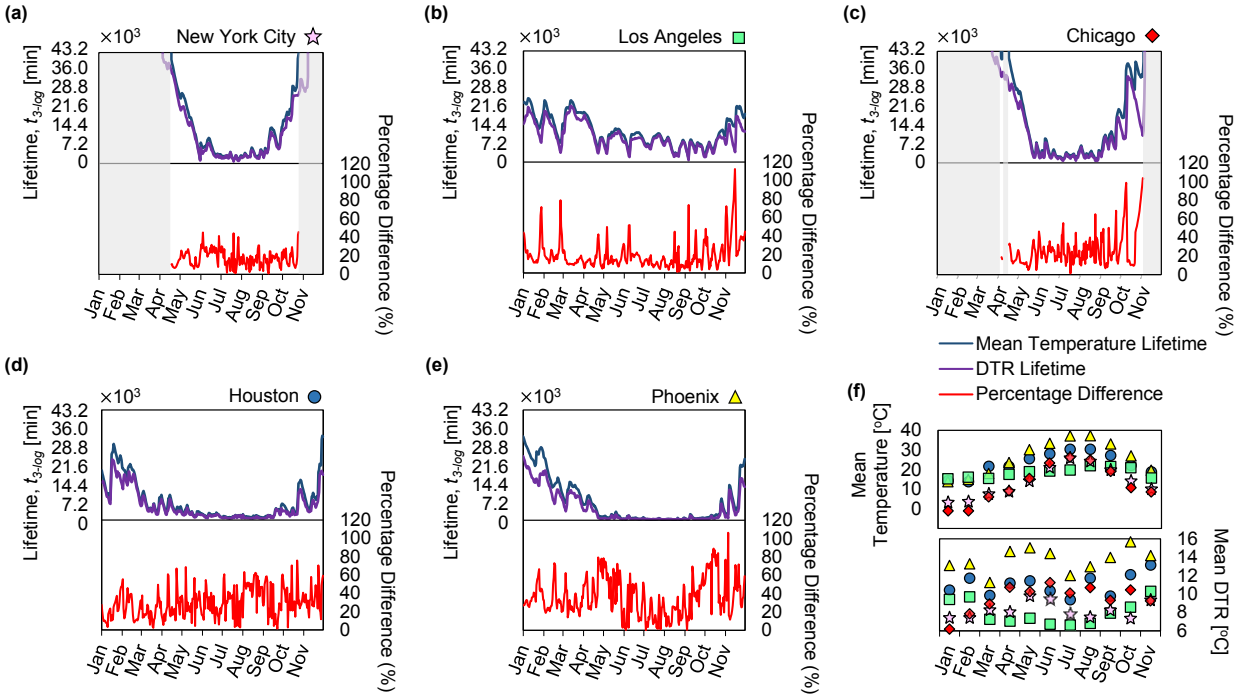

Figure 3 (Double Column). *Lifetime of SARS-CoV-2 and percentage difference between predictions using the simple daily mean temperature profile (blue line) versus the time-varying temperature profile (purple line) for the five most populous cities in the U.S. as reported by the U.S. Census Bureau: (a) New York City, (b) Los Angeles, (c) Chicago, (d) Houston, and (e) Phoenix. The plots show the predicted lifetime of SARS-CoV-2 for the months of January 2020 through November 2020. The mean temperature and DTR pertaining to each city averaged by month are plotted in (f) to illustrate climate trends in each city. The symbols correspond to (a)-(e). The lifetime axis is scaled to reflect 30 days (7.2×10^3 min = 5 days); predicted values for lifetimes greater than one month are not reported, and the corresponding periods of time are shaded in gray.*

in mean temperature throughout the year, exhibit correspondingly small variations in SARS-CoV-2 lifetime, whereas cities like New York City and Chicago show large variations in virus lifetime due to large variations in mean temperature throughout the year. We also observed that the percentage difference in lifetime predictions between the time-varying temperature profile and

daily mean temperature profile is relatively low for Los Angeles when compared to Phoenix, in this case due to the higher typical DTR experienced by Phoenix (2x the DTR of Los Angeles).

We studied the generalized effect of DTR on the lifetime of SARS-CoV-2 (for applicability to any city) by implementing a parametric sweep across both daily mean temperature and DTR (**Figure 4**), showing the predicted lifetime of the virus in **Figure 4(b)** and the percentage difference between the lifetimes calculated using the two different temperature profiles (simple daily mean versus time-varying) in **Figure 4(c)**. The time-varying temperature profile used to calculate the virus lifetime in **Figure 4(b)** maintains a fixed sunrise time at 0600 hours; a comparison of virus lifetime computed between varied and fixed sunrise time showed an average percentage difference of 0.68% across all five cities discussed above (Figure S6 in the Supplementary Material). The lifetime at each point on the heat map was computed by holding the daily mean temperature and DTR constant in the WAVE temperature profile. The computed lifetime becomes dependent on the starting time of the temperature profile at high mean temperature and high DTR due to shorter virus lifetimes (i.e., less than one day); modeling the virus lifetime starting from solar noon (at the maximum temperature) versus sunrise (at the minimum temperature) can yield an order of magnitude higher initial rate constant due to the exponential dependence on temperature. To overcome this issue and accommodate generalized results, the values presented in the heat maps are provided on an averaged basis, determined by taking the geometric mean of lifetimes starting every hour for a full diurnal temperature cycle; i.e., the values shown in the plots represent an average of 24 predicted lifetimes, each offset by one hour in starting time throughout a diurnal cycle. The percentage difference is then calculated by comparing the

averaged lifetimes determined using the time-varying temperature profile with those from the simple daily mean temperature profile.

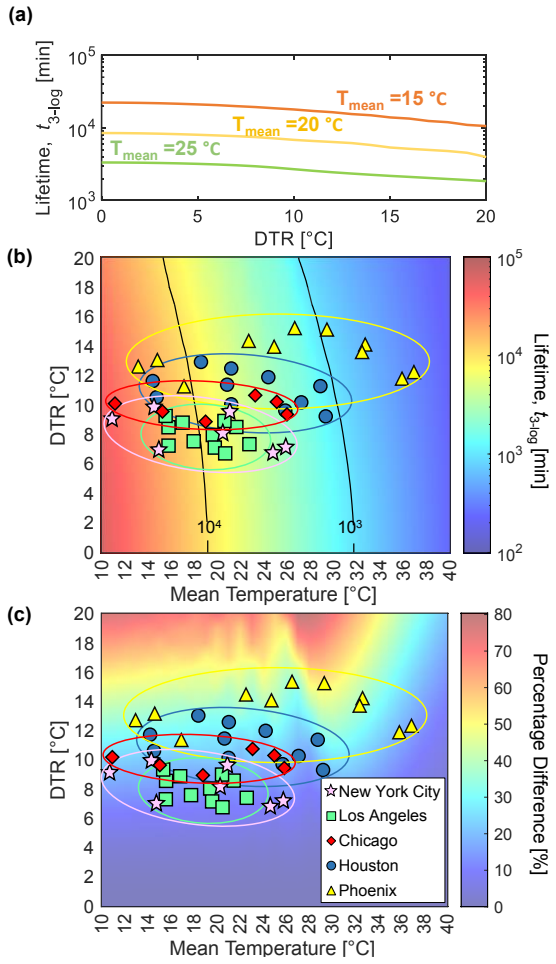

Figure 4 (Single Column). *The lifetime of SARS-CoV-2 varies with both the mean environmental temperature and the DTR. The lifetime of the virus is plotted against DTR for mean temperatures of 15, 20, and 25 °C to show that an increased DTR results in a shorter lifetime (a). A parametric sweep shows the lifetime of SARS-CoV-2 versus mean temperature and DTR (b), where increasing mean temperature and DTR both result in shorter virus lifetime. The percentage difference between predicted lifetime of SARS-CoV-2 calculated with the simple mean temperature profile versus lifetime calculated with the time-varying temperature profile accounting for DTR (c) shows that disparities between the two models are larger for higher values of DTR, with up to 50% deviation in lifetime due to DTR in some climates considering monthly averaged temperatures. The mean monthly DTR and mean temperatures for each city are overlaid to highlight trends of virus lifetime in cities with disparate climates. City-specific data points for months corresponding to mean temperatures less than 10 °C are not included.*

4. Discussion

As shown in **Figure 4(a)**, for a given daily mean temperature, the virus lifetime is shorter for regions with higher DTR. Cities like Los Angeles with relatively small temperature variations throughout the year see correspondingly small effects on virus lifetime, whereas cities like Phoenix, with both high DTR and large variations in mean temperature, exhibit a wider range of virus lifetimes spanning across the contour lines on the lifetime heat map throughout a year **(Figure 4(b))**. Cities like New York City and Chicago experience extreme cold temperatures in winter, resulting in virus lifetimes greater than one month, but as the environmental temperatures become warmer, virus lifetime drastically decreases. **Figure 4(c)** shows the percentage difference between predictions based on daily temperature fluctuations and those only considering daily mean temperatures. At DTR = 0, this plot shows predictions based only on the mean temperature; in this case, the percentage difference between the two models is effectively 0%. This heat map also shows where daily temperature fluctuations become important. For example, Phoenix typically has a high average monthly mean temperature and a large DTR, resulting in a high percentage difference (35–50%) between the two models. On the other hand, Los Angeles, with lower monthly mean temperatures and DTR, exhibits a relatively small percentage difference (10–20%). We also note that the day-to-day temperature variations could yield percentage differences as high as 120% (Figure 3b-d), further highlighting the influence DTR has on the prediction of virus lifetime across regions and illustrates that, as the DTR increases, the difference in predicted virus lifetime becomes more pronounced. For a given mean temperature, as the magnitude of DTR increases, the percentage difference between the two models becomes monotonically larger, signifying the importance of accounting for fluctuating environmental temperatures. This knowledge of how DTR influences virus lifetime becomes crucial when comparing policy decisions for cities or regions with similar daily mean temperatures but different DTR because they may experience disparate virus lifetimes.

The model presented in this work elucidates the independent effects of the magnitude of DTR and mean temperature on virus lifetime. This information could be of use when predicting the spread of the COVID-19 pandemic by providing a physical understanding of the effects of DTR, allowing epidemiologists to treat the environmental temperature variables independently. We note that reports in the literature using statistical analyses to study the correlation between various meteorological variables have considered DTR, and have found a negative correlation between the magnitude of DTR and number of cases of COVID-19. In one instance, Islam et al. studied the COVID-19 cases in seven climatic regions of Bangladesh from March to May 2020, and reported mean relative risk (RR) values of 0.95–0.97 as a function of increased DTR (with RR < 1 indicating that the risk of transmission is decreased) (Islam et al., 2020). Another study by Liu et al. reported a pooled RR of 0.9 for each 1 °C increase in the DTR for 30 cities in China from January 2020 to March 2020, and suggested that the viruses thrive in regions with low DTR or constant temperature (Liu et al., 2020). Recent studies on the number of COVID-19 cases in Indonesia, India, and Russia (the sub-arctic region) also reported negative correlations with DTR, all showing a similar trend despite representing vastly different regions of the world (Pramanik et al., 2020; Pratim, 2020; Supari et al., 2020). Prior work studying the dengue virus—an endemic virus in more than 100 countries—found that mosquitoes, the primary vector for transmission of the disease, are less susceptible to infection at high DTR, resulting in a lower rate of transmission of the disease (Ehelepola and Ariyaratne, 2016; Lambrechts et al., 2011); further investigation of the specifics of this vector of transmission in the context of DTR may be possible using our modeling framework. We also included Influenza A in **Figure 2** because Influenza A exhibits temperature-dependent inactivation (see Figure S6 in Supplementary Material). Several studies indicate a positive correlation between Influenza A transmission and DTR, but these studies also mention that large temperature fluctuations tend to lower the immune system and consequently increase the risk of infections (Park et al., 2020; Zhang et al., 2019), suggesting that a more

detailed statistical analysis would be needed to determine the isolated effect of DTR on transmission of Influenza A.

In the context of these findings, we emphasize that the purpose of the model presented here is to provide a fundamental understanding of the impact of realistic environmental temperature fluctuations on virus lifetime as compared to only considering mean daily temperatures. The model does not consider relative humidity, fomite material (i.e. the surface contaminated with a virus), or solar irradiation on exposed outdoor surfaces, all of which are known to affect virus lifetime (Carleton et al., 2021; Ficetola and Rubolini, 2021; McDevitt et al., 2010; van Doremalen et al., 2020; Zhang et al., 2020; Zhao et al., 2020). Relative humidity and fomite material can be treated as catalytic effects (Morris et al., 2020; Roduner, 2014) (among other mechanisms (Lin and Marr, 2020)), and adjustments to the activation energy could allow for additional predictive capabilities. Varying non-pharmaceutical intervention methods and social structures also play a role in the transmission of diseases and must be carefully accounted for when modelling the site-specific spread of the current pandemic (Bouchnita and Jebrane, 2020; Ficetola and Rubolini, 2021; Lin et al., 2020; Thu et al., 2020; Zhao et al., 2020). For simplicity and ease of comparison between the environmental temperatures of different cities, the temperature profiles used in this work are assumed to follow a smooth sinusoidal profile as described by the WAVE model; in reality, the actual temperature profiles are not smooth, and deviations from a sinusoidal profile may occur. Fortunately, specific regional environmental temperature can easily be incorporated into Eq. **4** in future work as *T(t).* Finally, we note that there are different methods to express time-varying temperature profiles; the WAVE profile was utilized in this study due to its simple, yet accurate, depiction of the diurnal temperature cycle, where prior work has shown that the WAVE model had an R^2 value of 0.95 compared to actual observed hourly temperature data and exhibited an absolute error of less than 3 °C (Baker et al., 1988; Cesaraccio et al., 2001; Reicosky et al., 1989). The lifetimes presented in **Figure 3** have been limited to a maximum of one month due to inherent uncertainties in predictions at colder

376 temperatures and longer times. In **Figure 4**, the lower limit of the daily mean temperature was
377 chosen as 10 ℃ because the lifetime at lower temperatures is greater than one month.
378
379 **5. Conclusions**
380 This study presents an analytical framework to understand the effects of temperature
381 fluctuations on virus lifetime. We show that regions with similar mean temperatures can potentially
382 exhibit a difference in virus lifetimes of greater than 50% when accounting for DTR, and day-to-
383 day temperature variations in a city could result in differences as large as 120%. Our model allows
384 for incorporation of realistic temperature profiles to predict the transmission of viruses, and could
385 therefore play a role in mitigating the spread of COVID-19. In addition, an array of mean
386 environmental temperature and DTR values were used to determine the virus lifetime and
387 highlight, for a given mean temperature, the magnitude of DTR at which temperature fluctuations
388 become significant in predicting virus lifetime. Finally, we show that the model can be adapted to
389 predict lifetimes and seasonal trends for other viruses—including, potentially, novel viruses that
390 have not yet been encountered—and used as a tool based on lab-scale experimental
391 characterization or simulation, rather than statistical analysis of transmission after a virus has
392 already become widespread. Ultimately, this work describes how time-varying environmental
393 temperature profiles result in shorter virus lifetime with a thermodynamic framework to bridge the
394 gap between statistical analyses and physical understanding.

Graphical Abstract

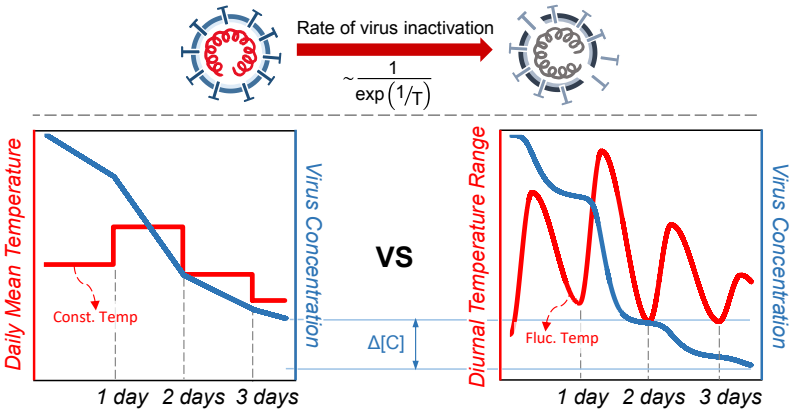

Acknowledgments

We gratefully acknowledge funding support from the National Science Foundation under Grant No. CBET-2030023, with Dr. Ying Sun as program director.

References

Abdelrahman, Z., Li, M., Wang, X., 2020. Comparative Review of SARS-CoV-2, SARS-CoV, MERS-CoV, and Influenza A Respiratory Viruses. Front. Immunol. 11. https://doi.org/10.3389/fimmu.2020.552909

Anver Sethwala, Mohamed Akbarally, Nathan Better, Jeffrey Lefkovits, Leeanne Grigg, H.A., 2020. The effect of ambient temperature on worldwide COVID-19 cases and deaths – an epidemiological study. medRxiv Prepr. 1–22. https://doi.org/10.1101/2020.05.15.20102798

Baker, J.M., Reicosky, D.C., Baker, D.G., 1988. Estimating the Time Dependence of Air Temperature Using Daily Maxima and Minima: A Comparison of Three Methods. J. Atmos. Ocean. Technol. 5, 736–742. https://doi.org/10.1175/1520-0426(1988)005<0736:ettdoa>2.0.co;2

Boone, S.A., Gerba, C.P., 2007. Significance of fomites in the spread of respiratory and enteric viral disease. Appl. Environ. Microbiol. 73, 1687–1696. https://doi.org/10.1128/AEM.02051-06

Bouchnita, A., Jebrane, A., 2020. A hybrid multi-scale model of COVID-19 transmission dynamics to assess the potential of non-pharmaceutical interventions. Chaos, Solitons and Fractals 138. https://doi.org/10.1016/j.chaos.2020.109941

Carleton, T., Cornetet, J., Huybers, P., Meng, K.C., Proctor, J., 2021. Global evidence for ultraviolet radiation decreasing COVID-19 growth rates. Proc. Natl. Acad. Sci. https://doi.org/10.1073/pnas.2012370118

CDC, 2008. Disinfection of Healthcare Equipment [WWW Document]. URL https://www.cdc.gov/infectioncontrol/guidelines/disinfection/healthcare-equipment.html

Cesaraccio, C., Spano, D., Duce, P., Snyder, R.L., 2001. An improved model for determining degree-day values from daily temperature data. Int. J. Biometeorol. 45, 161–169. https://doi.org/10.1007/s004840100104

Ehelepola, N.D.B., Ariyaratne, K., 2016. The correlation between dengue incidence and diurnal ranges of temperature of Colombo district, Sri Lanka 2005–2014. Glob. Health Action 9. https://doi.org/10.3402/gha.v9.32267

FDA, 2020a. Investigating Decontamination and Reuse of Respirators in Public Health Emergencies.

FDA, 2020b. Recommendations for Sponsors Requesting EUAs for Decontamination and Bioburden Reduction Systems for Face Masks and Respirators During the Coronavirus Disease 2019 (COVID-19) Public Health Emergency | FDA.

Ficetola, G.F., Rubolini, D., 2021. Containment measures limit environmental effects on COVID-19 early outbreak dynamics. Sci. Total Environ. 761, 144432. https://doi.org/10.1016/j.scitotenv.2020.144432

Firquet, S., Beaujard, S., Lobert, P.E., Sané, F., Caloone, D., Izard, D., Hober, D., 2015. Survival of enveloped and non-enveloped viruses on inanimate surfaces. Microbes Environ. 30, 140–144. https://doi.org/10.1264/jsme2.ME14145

Gao, C.X., Li, Y., Wei, J., Cotton, S., Hamilton, M., Wang, L., Cowling, B.J., 2021. Multi-route respiratory infection: When a transmission route may dominate. Sci. Total Environ. 752, 141856. https://doi.org/10.1016/j.scitotenv.2020.141856

Islam, A.R.M.T., Hasanuzzaman, M., Azad, M.A.K., Salam, R., Toshi, F.Z., Khan, M.S.I., Alam, G.M.M., Ibrahim, S.M., 2020. Effect of meteorological factors on COVID-19 cases in Bangladesh. Env. Dev Sustain. https://doi.org/10.1007/s10668-020-01016-1

Kampf, G., Todt, D., Pfaender, S., Steinmann, E., 2020. Persistence of coronaviruses on inanimate surfaces and their inactivation with biocidal agents. J. Hosp. Infect. 104, 246–251. https://doi.org/10.1016/j.jhin.2020.01.022

Kim, J., Shin, J., Lim, Y.H., Honda, Y., Hashizume, M., Guo, Y.L., Kan, H., Yi, S., Kim, H., 2016. Comprehensive approach to understand the association between diurnal temperature range and mortality in East Asia. Sci. Total Environ. 539, 313–321. https://doi.org/10.1016/j.scitotenv.2015.08.134

Lambrechts, L., Paaijmans, K.P., Fansiri, T., Carrington, L.B., Kramer, L.D., Thomas, M.B., Scott, T.W., 2011. Impact of daily temperature fluctuations on dengue virus transmission by Aedes aegypti. Proc. Natl. Acad. Sci. U. S. A. 108, 7460–7465. https://doi.org/10.1073/pnas.1101377108

Lin, C., Lau, A.K.H., Fung, J.C.H., Guo, C., Chan, J.W.M., Yeung, D.W., Zhang, Y., Bo, Y., Hossain, M.S., Zeng, Y., Lao, X.Q., 2020. A mechanism-based parameterisation scheme to investigate the association between transmission rate of COVID-19 and meteorological factors on plains in China. Sci. Total Environ. 737, 140348. https://doi.org/10.1016/j.scitotenv.2020.140348

Lin, K., Marr, L.C., 2020. Humidity-Dependent Decay of Viruses, but Not Bacteria, in Aerosols and Droplets Follows Disinfection Kinetics. Environ. Sci. Technol. 54, 1024–1032. https://doi.org/10.1021/acs.est.9b04959

Liu, J., Zhou, J., Yao, J., Zhang, X., Li, L., Xu, X., He, X., Wang, B., Fu, S., Niu, T., Yan, J., Shi, Y., Ren, X., Niu, J., Zhu, W., Li, S., Luo, B., Zhang, K., 2020. Impact of meteorological factors on the COVID-19 transmission: A multi-city study in China. Sci. Total Environ. 726, 138513. https://doi.org/10.1016/j.scitotenv.2020.138513

Luo, Y., Zhang, Y., Liu, T., Rutherford, S., Xu, Y., Xu, X., Wu, W., Xiao, J., Zeng, W., Chu, C., Ma, W., 2013. Lagged Effect of Diurnal Temperature Range on Mortality in a Subtropical Megacity of China. PLoS One 8. https://doi.org/10.1371/journal.pone.0055280

Ma, Y., Zhao, Y., Liu, J., He, X., Wang, B., Fu, S., Yan, J., Niu, J., 2020. Effects of temperature variation and humidity on the death ofCOVID-19 in Wuhan, China. Sci. Total Environ. 724. https://doi.org/10.1016/j.scitotenv.2020.138226

475 Malki, Z., Atlam, E.S., Hassanien, A.E., Dagnew, G., Elhosseini, M.A., Gad, I., 2020.
476 Association between weather data and COVID-19 pandemic predicting mortality rate:
477 Machine learning approaches. Chaos, Solitons and Fractals 138, 110137.
478 https://doi.org/10.1016/j.chaos.2020.110137
479 McDevitt, J., Rudnick, S., First, M., Spengler, J., 2010. Role of absolute humidity in the
480 inactivation of influenza viruses on stainless steel surfaces at elevated temperatures. Appl.
481 Environ. Microbiol. 76, 3943–3947. https://doi.org/10.1128/AEM.02674-09
482 Merow, C., Urban, M.C., 2020. Seasonality and uncertainty in global COVID-19 growth rates.
483 Proc. Natl. Acad. Sci. 202008590. https://doi.org/10.1073/pnas.2008590117
484 Morris, D.H., Yinda, K.C.H., Gamble, A., Rossine, F.W., Huang, Q., Bushmaker, T., Fischer,
485 R.J., Matson, M.J., Doremalen, N. van, Vikesland, P.J., Marr, L.C., Munster, V., Lloyd-
486 Smith, J.O., 2020. Mechanistic theory predicts the effects of temperature and humidity on
487 inactivation of SARS-CoV-2 and other enveloped viruses. bioRxiv 1–24.
488 Oral, E., Wannomae, K.K., Connolly, R., Gardecki, J., Leung, H.M., Muratoglu, O., Griffiths, A.,
489 Honko, A.N., Avena, L.E., Mckay, L.G.A., Flynn, N., Storm, N., Downs, S.N., Jones, R.,
490 Emmal, B., 2020. Vapor H 2 O 2 sterilization as a decontamination method for the reuse of
491 N95 respirators in the COVID-19 emergency 4, 1–5.
492 https://doi.org/10.1101/2020.04.11.20062026
493 Park, J.E., Son, W.S., Ryu, Y., Choi, S.B., Kwon, O., Ahn, I., 2020. Effects of temperature,
494 humidity, and diurnal temperature range on influenza incidence in a temperate region.
495 Influenza Other Respi. Viruses 14, 11–18. https://doi.org/10.1111/irv.12682
496 Pirouz, Behzad, Golmohammadi, A., Saeidpour Masouleh, H., Violini, G., Pirouz, Behrouz,
497 2020. Relationship between Average Daily Temperature and Average Cumulative Daily
498 Rate of Confirmed Cases of COVID-19. medRxiv.
499 https://doi.org/10.1101/2020.04.10.20059337
500 Pramanik, M., Udmale, P., Bisht, P., Chowdhury, K., Szabo, S., Pal, I., 2020. Climatic factors

influence the spread of COVID-19 in Russia. Int. J. Environ. Health Res. 1–16. https://doi.org/10.1080/09603123.2020.1793921

Pratim, R.M., 2020. Impact of Temperature on Covid 19 in India. medRxiv. https://doi.org/10.1101/2020.08.30.20184754

Rahman, M.A., Hossain, M.G., Singha, A.C., Islam, M.S., Islam, M.A., 2020. A Retrospective Analysis of Influence of Environmental/Air Temperature and Relative Humidity on Sars-CoV-2 Outbreak. J. Pure Appl. Microbiol. 14, 1705–1714. https://doi.org/10.22207/jpam.14.3.09

Reicosky, D.C., Winkelman, L.J., Baker, J.M., Baker, D.G., 1989. Accuracy of Hourly Air Temperatures Calculated from Daily Minima and Maxima. Agric. For. Meteorol. 46, 193–209. https://doi.org/10.1016/0168-1923(89)90064-6

Roduner, E., 2014. Understanding catalysis. Chem. Soc. Rev. 43, 8226–8239. https://doi.org/10.1039/c4cs00210e

Sajadi, M.M., Habibzadeh, P., Vintzileos, A., Shokouhi, S., Miralles-Wilhelm, F., Amoroso, A., 2020. Temperature, Humidity, and Latitude Analysis to Estimate Potential Spread and Seasonality of Coronavirus Disease 2019 (COVID-19). JAMA Netw. open 3, e2011834. https://doi.org/10.1001/jamanetworkopen.2020.11834

Supari, S., Nuryanto, D.E., Setiawan, A.M., Sopaheluwakan, A., Alfahmi, F., Hanggoro, W., Gustari, I., Safril, A., Yunita, R., 2020. The association between Covid19 data and meteorological factors in Indonesia. Res. Sq. 1–25.

Thu, T.P.B., Ngoc, P.N.H., Hai, N.M., Tuan, L.A., 2020. Effect of the social distancing measures on the spread of COVID-19 in 10 highly infected countries. Sci. Total Environ. 742, 140430. https://doi.org/10.1016/j.scitotenv.2020.140430

van Doremalen, N., Bushmaker, T., Morris, D.H., Holbrook, M.G., Gamble, A., Williamson, B.N., Tamin, A., Harcourt, J.L., Thornburg, N.J., Gerber, S.I., Lloyd-Smith, J.O., de Wit, E., Munster, V.J., 2020. Aerosol and Surface Stability of SARS-CoV-2 as Compared with

527 SARS-CoV-1. N. Engl. J. Med. https://doi.org/10.1056/NEJMc2004973
528 Xiao, S., Li, Y., Wong, T. wai, Hui, D.S.C., 2017. Role of fomites in SARS transmission during
529 the largest hospital outbreak in Hong Kong. PLoS One 12, 1–13.
530 https://doi.org/10.1371/journal.pone.0181558
531 Yap, T.F., Liu, Z., Shveda, R.A., Preston, D.J., 2020. A predictive model of the temperature-
532 dependent inactivation of coronaviruses. Appl. Phys. Lett. 117.
533 https://doi.org/10.1063/5.0020782
534 Yeo, C., Kaushal, S., Yeo, D., 2020. Enteric involvement of coronaviruses: is faecal–oral
535 transmission of SARS-CoV-2 possible? Lancet Gastroenterol. Hepatol. 5, 335–337.
536 https://doi.org/10.1016/S2468-1253(20)30048-0
537 Zhang, A.L., Wang, Y., Molina, M.J., 2020. Correction for Zhang et al., Identifying airborne
538 transmission as the dominant route for the spread of COVID-19. Proc. Natl. Acad. Sci. 117,
539 25942–25943. https://doi.org/10.1073/pnas.2018637117
540 Zhang, Y., Ye, C., Yu, J., Zhu, W., Wang, Y., Li, Z., Xu, Z., Cheng, J., Wang, N., Hao, L., Hu,
541 W., 2019. The complex associations of climate variability with seasonal influenza A and B
542 virus transmission in subtropical Shanghai, China. Sci. Total Environ. 701, 1–9.
543 https://doi.org/10.1016/j.scitotenv.2019.134607
544 Zhao, L., Qi, Y., Luzzatto-Fegiz, P., Cui, Y., Zhu, Y., 2020. COVID-19: Effects of Environmental
545 Conditions on the Propagation of Respiratory Droplets. Nano Lett. 20, 7744–7750.
546 https://doi.org/10.1021/acs.nanolett.0c03331
547 Zhu, Z., Lian, X., Su, X., Wu, W., Marraro, G.A., Zeng, Y., 2020. From SARS and MERS to
548 COVID-19: A brief summary and comparison of severe acute respiratory infections caused
549 by three highly pathogenic human coronaviruses. Respir. Res. 21, 1–14.
550 https://doi.org/10.1186/s12931-020-01479-w

Table 1. Activation energy and frequency factor values used to determine virus lifetime. Values for coronaviruses were determined in prior work (Yap et al., 2020). Primary datasets used to obtain activation energy and frequency factor for Influenza A are provided in the Supplementary Material.

	Activation Energy, E_a [kJ/mol]	**Frequency Factor, ln(A) [1/min]**
SARS-CoV-2	135.7	48.6
SARS-CoV-1	142.6	51.9
MERS-CoV	135.4	49.5
Influenza A	41.0	12.2

Supplementary Material for

Effect of Daily Temperature Fluctuations on Virus Lifetime

Te Faye Yap,[1] Colter J. Decker,[1] Daniel J. Preston[1,*]

[1]Deptartment of Mechanical Engineering, Rice University, 6100 Main St., Houston, TX 77005

*To whom correspondence should be addressed

Phone: 713-348-4642

Email: djp@rice.edu

Other supplementary materials for this manuscript include the following:

Datasets S1 and S2 [Available upon request: djp@rice.edu]

Supplementary Text

Numerical Analysis

Due to the dependence of temperature on time following the WAVE profile, the integral shown in Eq. **4** in the main text cannot be solved analytically. Euler's method is used to determine the concentration of virus at a given time for a given temperature profile, $T(t)$. Eq. **S1** through **S3** show the steps used to solve for the concentration after a given time step:

$$\int_{[C]_0}^{[C]} \frac{d[C]}{[C]} = \int_{t_0}^{t} -A \exp\left(-\frac{E_a}{RT(t)}\right) dt \qquad \text{[Eq. S1]}$$

$$\frac{[C]_{i+1} - [C]_i}{dt} = -A \exp\left(-\frac{E_a}{RT(t)}\right) [C]_i \qquad \text{[Eq. S2]}$$

$$[C]_{i+1} = -A \exp\left(-\frac{E_a}{RT(t)}\right) [C]_i \, dt + [C]_i \qquad \text{[Eq. S3]}$$

where i represents the number of time steps needed to determine the viable virus concentration. At $t = 0$, $i = 0$, corresponding to the initial virus concentration, $[C]_0$. The vertical axis in **Figure 2** in the main text is plotted in terms of an n-log reduction. This value is determined by taking the ratio between the concentration at a given time, $[C]$, and the initial concentration, $[C]_0$, in terms of orders of magnitude (the base-10 logarithm of the ratio):

$$n = log_{10} \frac{[C]}{[C]_0} \qquad \text{[Eq. S4]}$$

Quantitative Understanding of the Effects of DTR

We show that the virus concentration will always be lesser when taking into account the diurnal temperature range (DTR) compared to the case considering only mean temperature (**Figure S1(A)**). By evaluating the change in concentration over an infinitesimally small timestep

(**Figure S1(B)**)**,** we can treat the local time-varying temperature profile as a step function, with Δ*T* representing an arbitrary temperature variation from the mean. To prove that the change in concentration, Δ[*C*] (i.e., the final concentration minus the initial concentration) when accounting for DTR will be lesser (more negative) than when only considering the mean temperature over a given timestep, we start by assigning an inequality corresponding to our hypothesis:

$$\Delta[C]_{mean} > \Delta[C]_{DTR} \qquad \text{[Eq. } \mathbf{S5}\text{]}$$

The Δ[*C*] is more negative for a greater magnitude of decrease in concentration, so the Δ[*C*] considering DTR will be less than the Δ[*C*] based on the mean temperature if temperature fluctuations result in a larger decrease in concentration. Based on the rate law for a first-order reaction, d[*C*]/dt = *C'*, which is also a function of temperature, *T*, the change in concentration is over an infinitesimally small timestep is:

$$\Delta[C] = C'(T)\Delta t \qquad \text{[Eq. } \mathbf{S6}\text{]}$$

Substituting Eq. **S6** into Eq. **S5** and multiplying by the relevant timesteps shown in **Figure S1(B)** to determine the concentration, we obtain:

$$C'(T)(p+q)\Delta t > C'(T+p\Delta T)(q\Delta t) + C'(T-q\Delta T)(p\Delta t) \qquad \text{[Eq. } \mathbf{S7}\text{]}$$

where *p* and *q* are numbers between 0 and 1 that sum to 1 (i.e., *p* + *q* = 1). We assign these *p* and *q* parameters to allow for a more general consideration of any asymmetric temperature profile for which the average of the temperature variations over a given timestep is equal to the mean temperature (**Figure S1(C)**). At the limiting case where *p* = 1 and *q* = 0 (or vice versa), the profile is equivalent to the mean temperature case.

Any arbitrary time-varying temperature profile *T*(*t*) can be constructed from a sum of many of these timesteps; therefore, by showing that this temperature profile with temperature fluctuations always results in a larger decrease in concentration than the mean temperature profile at every timestep, the result can be extended to any time-varying temperature profile *T*(*t*), including the temperature profile accounting for DTR in this work.

We take a second-order Taylor series expansion for a case with small temperature variations above and below the mean:

$$C'(T + p\Delta T) = C'(T) + \frac{dC'(T)}{dT}(p\Delta T) + \frac{1}{2}\frac{d^2C'(T)}{dT^2}(p\Delta T)^2 \quad \text{[Eq. S8]}$$

$$C'(T - q\Delta T) = C'(T) - \frac{dC'(T)}{dT}(q\Delta T) + \frac{1}{2}\frac{d^2C'(T)}{dT^2}(q\Delta T)^2 \quad \text{[Eq. S9]}$$

We substitute the second-order Taylor series expansion into Eq. **S7** to obtain:

$$C'(T)\Delta t > C'(T)\Delta t + \frac{d^2C'(T)}{dT^2}\frac{pq\Delta t\Delta T^2}{2} \quad \text{[Eq. S10]}$$

When $\Delta T = 0$, we see that the both sides of the inequality are equal, recovering the original form when only considering mean temperatures. In order for this inequality to hold true, the second term on the right-hand side must always be negative.

$$\frac{d^2C'(T)}{dT^2}\frac{pq\Delta t\Delta T^2}{2} < 0 \quad \text{[Eq. S11]}$$

Since *p, q,* ΔT*,* and Δt are always positive, we focus on expanding the second order differential equation for *C*' by substituting the Arrhenius equation (Eq. S**18**):

$$\frac{d^2}{dT^2}\left(-Aexp\left(-\frac{E_a}{RT}\right)C_0\right) < 0 \quad \text{[Eq. S12]}$$

Taking the first derivative with respect to temperature:

$$\frac{d}{dT}\left(-\frac{AC_0E_a}{R}exp\left(-\frac{E_a}{RT}\right)\frac{1}{T^2}\right) < 0 \quad \text{[Eq. S13]}$$

Taking the second derivative with respect to temperature:

$$-\frac{AC_0E_a^2}{R^2}exp\left(-\frac{E_a}{RT}\right)\frac{1}{T^4} + \frac{2AC_0E_a}{R}exp\left(-\frac{E_a}{RT}\right)\frac{1}{T^3} < 0 \quad \text{[Eq. S14]}$$

After simplifying Eq. **S14**, the criterion for $\Delta[C]_{mean} > \Delta[C]_{DTR}$ is:

$$\frac{1}{2}\frac{E_a}{RT} > 1 \qquad \text{[Eq. } \mathbf{S15}\text{]}$$

In order to demonstrate that the inequality holds true for all relevant temperature conditions, we determined "worst-case scenario" values for the left-hand side of the inequality for the viruses studied in this work at the highest environmental temperature ever recorded on Earth (58 °C in El Azizia, Libya (Mildrexler et al., 2006)) to obtain conservative estimates (Table **S1**). We show that these values are always much greater than 1, demonstrating that fluctuating temperatures will always reduce virus lifetime compared to the corresponding mean temperature for the viruses studied here at any environmentally relevant conditions.

In fact, considering the case for Influenza A, the absolute temperature would need to be 7.5 times greater than the current characteristic environmental temperature (i.e., greater than ~2500 K) for the inequality to break down. Under all relevant environmental temperatures, the activation energy is much greater than the thermal energy. When comparing the Arrhenius equation with the Eyring equation, we also observe that the activation energy is approximately equal to the activation enthalpy, $\Delta H^{\ddagger}$, at environmental temperatures (i.e., the RT term is negligible in Eq. **S16**):

$$E_a = \Delta H^{\ddagger} + RT \qquad \text{[Eq. } \mathbf{S16}\text{]}$$

We plotted the concentration of virus (Eq. **S3**) after a given timestep and compared the relative degree of inactivation when considering a fluctuating temperature profile to the case considering only the mean temperature to illustrate that the magnitude of change in concentration is always greater for the case of the fluctuating temperature profile (Eq. **S5**). The relative *n*-log reduction (where the value of *n* corresponds to the order-of-magnitude degree of inactivation) is defined as:

$$\frac{n_{DTR}}{n_{mean}} = \frac{log_{10}\frac{[C]_{DTR}}{[C]_i}}{log_{10}\frac{[C]_{mean}}{[C]_i}} \qquad \text{[Eq. } \mathbf{S17}\text{]}$$

We plotted the relative *n*-log reduction against the value of *p* at a mean temperature of 20 °C for ΔT values of 5, 10, 15, and 20 °C **(Figure S1(D))**; the plot shows that considering

fluctuations in temperature (such as DTR) will always serve to increase degree of inactivation, in turn resulting in a lower virus concentration. This trend illustrates that the inequality hypothesized in Eq. **S5** holds true. **Figure S1(D)** also shows that for a higher ΔT, a higher rate of inactivation can occur when temperature fluctuations above the mean are higher, but for a shorter time period (i.e., $p > q$). At ΔT = 20 °C, we observe a fourfold increase in the relative n-log reduction of virus (i.e., 10,000x decrease in concentration) as compared to the mean temperature case when $p \approx 0.8$, highlighting the exponential dependence of virus lifetime on temperature. From this quantitative approach, the duration and magnitude of temperature variations from the mean are shown to play a critical role in the degree of virus inactivation.

Temperature Profile

In **Figures 3** and **4** in the main text, the WAVE temperature profile is used to model daily environmental temperature fluctuations. In **Figure 3**, the sunrise time (**Dataset S2**) used to generate the temperature profile corresponds to each city shown. However, for the heat map shown in **Figure 4**, a more general temperature profile is used, in which the sunrise time is fixed at 0600 hours. Fixing the sunrise time has a negligible effect on the resulting computed virus lifetimes. The virus lifetimes in the five major cities studied in this work were determined using both city-specific sunrise times and an 0600 fixed sunrise time, with the average percentage difference for all cities between these two methods being 0.68% (**Figure S8**).

Influenza A Inactivation Data

Data on the inactivation of influenza virus (A/Puerto Rico/8/34/H1N1 strain) in terms of time required to achieve n-log reduction for a given temperature were obtained from Greatorex et al. (Greatorex et al., 2011). The data presented in their work corresponds to the inactivation of H1N1 on a fomite of stainless steel. The authors report experimental conditions with temperatures ranging from 17–21 °C; we used an intermediate value of 19 °C in our work. The relative humidity reported in their work was 23 – 24 %. The natural logarithm of 10^{-n} was plotted against time following the linearized rate law for a first-order reaction (Eq. **1**), and the time scale was converted to minutes according to convention. A linear fit for the data at 19 °C is presented in **Figure S2**. The resulting slope was used to determine the rate constant at this temperature, reported in **Table S2**.

We followed the same procedure to homogenize data on influenza virus (A/PR/8/34 H1N1 strain) reported by McDevitt et al. (McDevitt et al., 2010) for H1N1 on a fomite of stainless steel. Linear fits for data at 55, 60, and 65 °C at a relative humidity of 25% are presented in **Figures S3** through **S5**. The resulting slopes were used to determine the rate constants at these temperatures, reported in **Table S2**.

Influenza A Temperature-Dependent Inactivation

According to the rate law for a first-order reaction (Eq. **1**), the rate constant, k, can be determined for the inactivation of a virus at a given temperature, T, by applying a linear regression and calculating the slope, $k = -\Delta\ln([C])/\Delta t$. Each pair of k and T determined from the primary data is plotted according to the linearized Arrhenius equation (Eq. **S7**) and yields a linear relationship between $\ln(k)$ and $1/T$ (**Figure S6**). The slope and intercept of the linear fit correspond to the activation energy, E_a, and log of frequency factor, $\ln(A)$. The log of frequency factor, $\ln(A)$, is plotted against activation energy, E_a, for the viruses considered in this work; the linear correlation between $\ln(A)$ and E_a indicates that the viruses undergo a thermal denaturation process following the Meyer-Neldel rule, supporting our hypothesis that the viruses are inactivated due to the thermal denaturation of proteins that comprise each virion (**Figure S7**). The linear regression calculated in this work after including influenza A, [$\ln(A) = 0.394E_a - 5.63$], is similar to the linear regression tabulated in previous work for only coronaviruses (Yap et al., 2020), and is nearly identical to those calculated in two prior studies on the denaturation of tissues and cells, which report [$\ln(A) = 0.380E_a - 5.27$] (Qin et al., 2014) and [$\ln(A) = 0.383E_a - 5.95$] (Wright, 2003).

$$\ln(k) = -\frac{E_a}{RT} + \ln(A) \qquad \text{[Eq. S18]}$$

Temperature Data

The temperature data for the five most populous cities in the United States from January 1, 2020, to December 29, 2020, were obtained from the National Oceanic and Atmospheric Administration (NOAA) climate data online search database. Temperature data from weather stations located at the major airports in each city were used in this work, i.e., JFK International Airport (New York City), Los Angeles International Airport (Los Angeles), Chicago O'Hare International Airport (Chicago), George Bush Intercontinental Airport (Houston), and Phoenix Sky Harbor Airport (Phoenix). The complete temperature dataset is included as **Dataset S1**.

Sunrise Time Data

The sunrise times used to determine the time periods of the half-cosine functions in the temperature profiles for the five most populous cities in the United States from January 1, 2020, to December 29, 2020, were obtained from the National Oceanic and Atmospheric Administration (NOAA) solar calculator. The complete dataset is included as **Dataset S2**; the highlighted rows and columns were adjusted for daylight saving time (note that Phoenix does not observe daylight saving time).

Fixed Sunrise Time (0600 hours) versus City-Specific Sunrise Time

The percentage difference in results when fixing the sunrise time at 0600 hours in the model versus assigning the actual sunrise time for each specific region is plotted in **Figure S9**. The low percentage difference (0.68% on average) allowed us to neglect the effect of region-specific sunrise time, and a fixed sunrise time at 0600 hours was used in the model to calculate the lifetimes displayed in the parametric sweep shown in **Figure 4** of the main text.

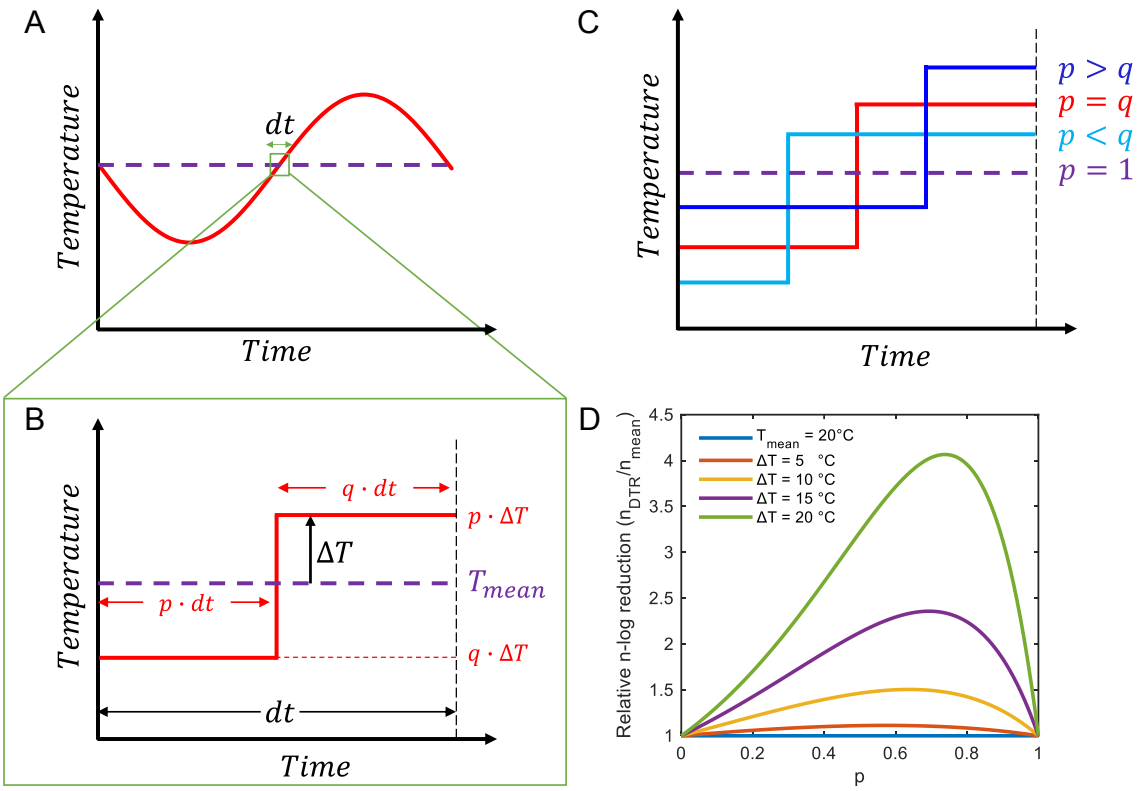

Fig. S1. (A) Sinusoidal temperature profile used to model temperature variations around the mean temperature. (B) Considering the temperature profile at a small timestep, the temperature profile can be approximated as a step function. The variables *p* and *q* are introduced to analyze cases where the temperature profile is not symmetric, but the average of this temperature profile is always equal to the mean temperature; *p* and *q* are positive numbers and *p* + *q* = 1. (C) Illustration of potential temperature profiles for different values of p. (D) The *n*-log reduction of virus inactivation when considering DTR, n_{DTR}, relative to the n-log reduction of virus when only considering mean temperatures, n_{mean}, against an array of p values varying from 0 to 1. The graph is plotted for a mean temperature of 20 °C and Δ*T* values of 5, 10, 15, and 20 °C to demonstrate the importance of considering DTR.

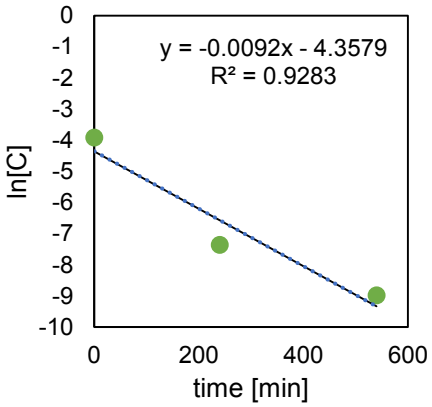

Fig. S2. Primary data from Greatorex et al. (Greatorex et al., 2011) for inactivation of H1N1 at 19 °C after converting the *n*-log reduction values from base-10 logarithm to natural log. We fit a line to the data to determine the rate constant at 19 °C.

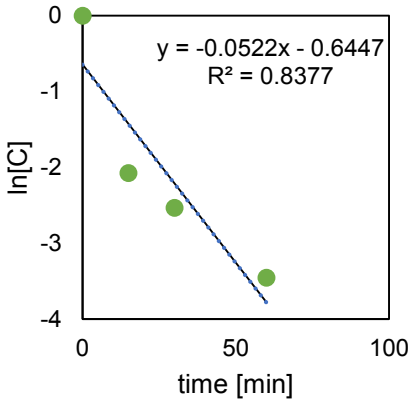

Fig. S3. Primary data from McDevitt et al. (McDevitt et al., 2010) for inactivation of H1N1 at 55 °C after converting the *n*-log reduction values from base-10 logarithm to natural log. We fit a line to the data to determine the rate constant at 55 °C.

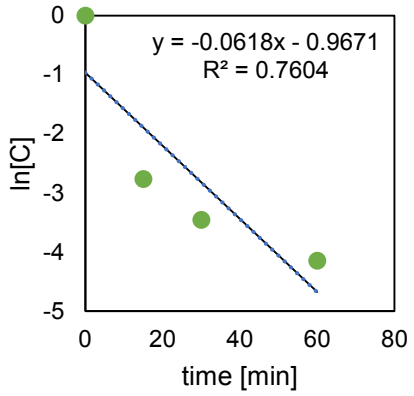

Fig. S4. Primary data from McDevitt et al. (McDevitt et al., 2010) for inactivation of H1N1 at 60 °C after converting the *n*-log reduction values from base-10 logarithm to natural log. We fit a line to the data to determine the rate constant at 60 °C.

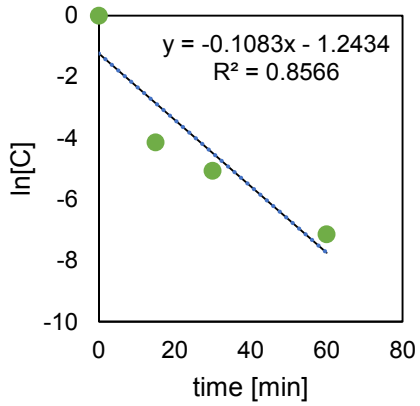

Fig. S5. Primary data from McDevitt et al. (McDevitt et al., 2010) for inactivation of H1N1 at 65 °C after converting the *n*-log reduction values from base-10 logarithm to natural log. We fit a line to the data to determine the rate constant at 65 °C.

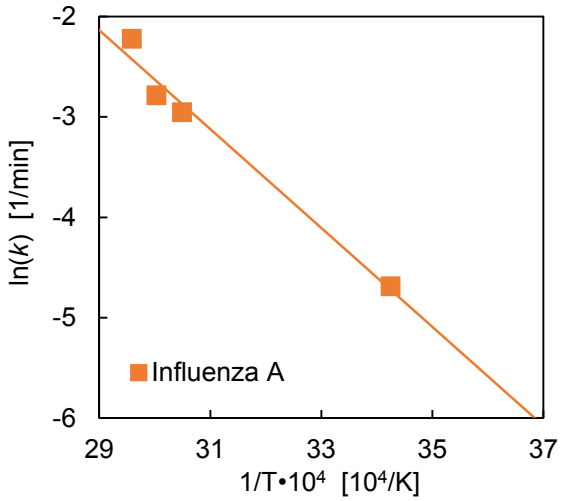

Fig. S6. From the Influenza A virus dataset, the rate constant, k, for a given temperature was found using linear regression according to Eq. **S5**. The slope and intercept of the linear fit correspond to the activation energy, E_a, and frequency factor, ln(A), for Influenza A.

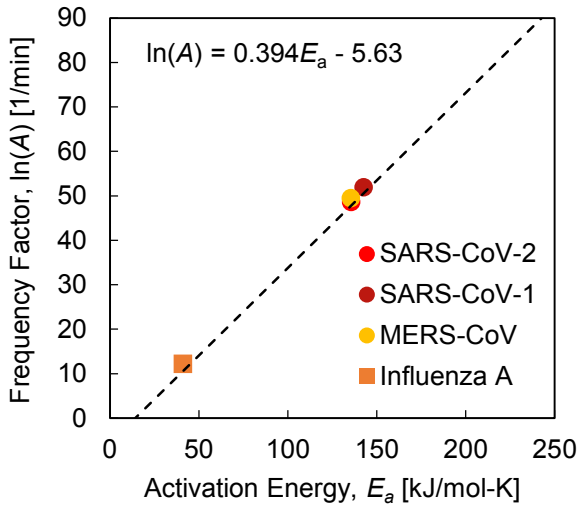

Fig. S7. Thermal inactivation parameters governing the inactivation behavior of SARS-CoV-2, SARS-CoV-1, MERS-CoV, and Influenza A. The frequency factor, ln(A), is plotted against the activation energy, E_a, according to the linearized Arrhenius equation; the linear correlation indicates protein denaturation following the Meyer-Neldel rule.

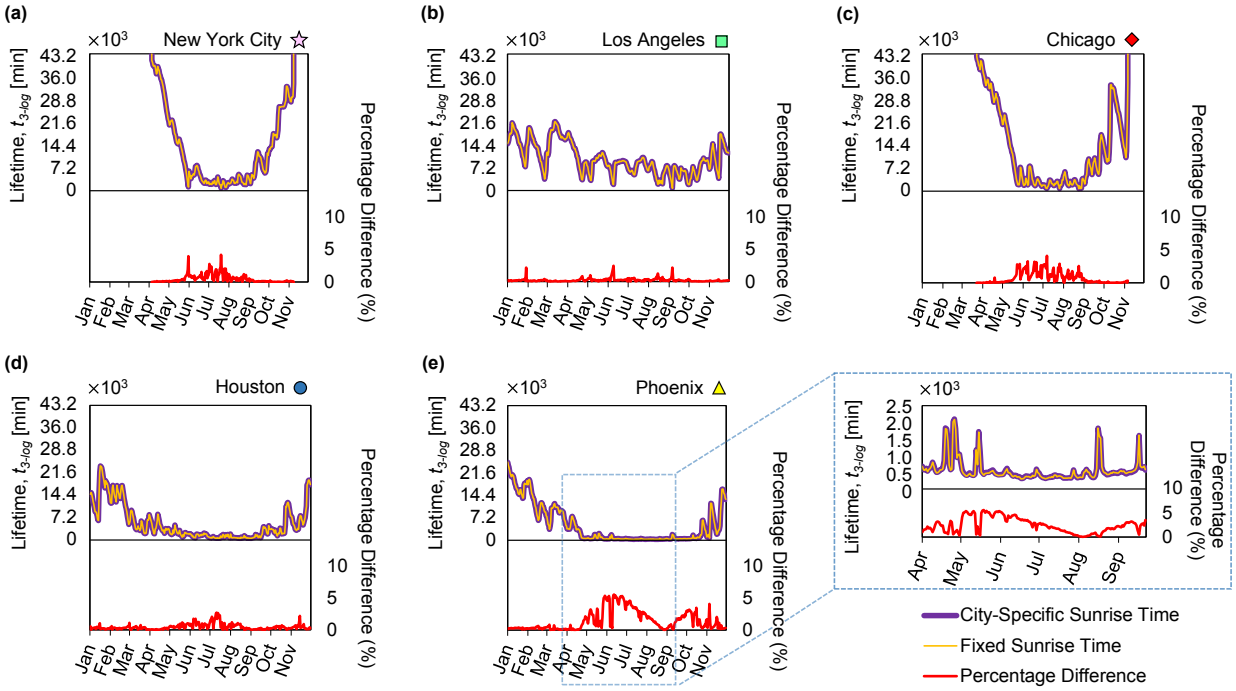

Fig. S8. The predicted lifetimes (7.2×10^3 min = 5 days) of SARS-CoV-2 for the months of January 2020 to November 2020, along with the percentage difference using city-specific and fixed (0600 hours) sunrise times, are plotted for (a) New York City, (b) Los Angeles, (c) Chicago, (d) Houston, and (e) Phoenix. The average percentage difference between these methods for all cities is 0.68%. Phoenix experiences the highest percentage difference of 5.55%. The region with this high percentage difference, from April to September 2020, is magnified to show the difference in lifetimes, which is likely due to a higher rate of inactivation at the higher overall temperatures in Phoenix during these months, highlighting the importance of the period of time between sunrise and solar noon during high environmental temperatures.

Table S1: Values for the left-hand side of Eq. **S13** to prove the inequality. Temperature was chosen as a conservative estimate for the maximum temperature attainable on Earth.

	Activation Energy, E_a [kJ/mol]	*E_a/2RT (Eq. **S13**)*
SARS-CoV-2	135.7	24.7 >> 1
SARS-CoV-1	142.6	25.9 >> 1
MERS-CoV	135.4	24.6 >> 1
Influenza A	41.0	7.5 >> 1

Table S2. Data for Influenza A obtained from Figures S2-5 and plotted in Figure S6 and data for SARS-CoV-2, SARS-CoV, and MERS-CoV from prior work (Yap et al., 2020)

Dataset	**SI Ref.**	**T [°C]**	**$1/T \cdot 10^4$ [10^4/K]**	**k = -d(ln[C])/dt [1/min]**	**ln(*k*) [1/min]**
Influenza A	(Greatorex et al., 2011)	19	34.25	0.0092	-4.689
Influenza A	(McDevitt et al., 2010)	55	30.49	0.0522	-2.953
Influenza A	(McDevitt et al., 2010)	60	30.03	0.0618	-2.784
Influenza A	(McDevitt et al., 2010)	65	29.59	0.1083	-2.223
SARS-CoV-2	(Chin et al., 2020)	4	36.10	0.0000597	-9.726
SARS-CoV-2	(Chin et al., 2020)	22	33.90	0.000696	-7.270
SARS-CoV-2	(van Doremalen et al., 2020)	22	33.90	0.00166	-6.401
SARS-CoV-2	(Chin et al., 2020)	37	32.36	0.00557	-5.190
SARS-CoV-2	(Chin et al., 2020)	56	30.39	0.724	-0.323
SARS-CoV-2	(Chin et al., 2020)	70	29.15	3.36	1.212
SARS-CoV-1	(van Doremalen et al., 2020)	22	33.90	0.00191	-6.261
SARS-CoV-1	(Darnell and Taylor, 2006)	56	30.40	0.9077	-0.097
SARS-CoV-1	(Darnell and Taylor, 2006)	65	29.59	2.869	1.054
MERS-CoV	(van Doremalen et al., 2013)	20	34.13	0.0027	-5.914
MERS-CoV	(Leclercq et al., 2014)	56	30.40	0.16	-0.999
MERS-CoV	(Leclercq et al., 2014)	65	29.59	3.62	2.121

Table S3. Experimental conditions at which E_a and ln(A) are determined for the viruses analyzed in this work.

Dataset	Ref.	T [°C]	Fomite	RH
SARS-CoV-2	(Chin et al., 2020)	4	Virus transport Medium	Not reported
SARS-CoV-2	(Chin et al., 2020)	22	Virus transport medium	Not reported
SARS-CoV-2	(van Doremalen et al., 2020)	22	Plastic	40%
SARS-CoV-2	(Chin et al., 2020)	37	Virus transport medium	Not reported
SARS-CoV-2	(Chin et al., 2020)	56	Virus transport medium	Not reported
SARS-CoV-2	(Chin et al., 2020)	70	Virus transport medium	Not reported
SARS-CoV-1	(van Doremalen et al., 2020)	22	Plastic	40%
SARS-CoV-1	(Darnell and Taylor, 2006)	56	Human serum	Not reported
SARS-CoV-1	(Darnell and Taylor, 2006)	65	Human serum	Not reported
MERS-CoV	(van Doremalen et al., 2013)	20	Plastic	40%
MERS-CoV	(Leclercq et al., 2014)	56	Modified Eagle's medium	Not reported
MERS-CoV	(Leclercq et al., 2014)	65	Modified Eagle's medium	Not reported
Influenza A	(Greatorex et al., 2011)	19	Stainless steel	23-24%
Influenza A	(McDevitt et al., 2010)	55	Stainless steel	25%
Influenza A	(McDevitt et al., 2010)	60	Stainless steel	25%
Influenza A	(McDevitt et al., 2010)	65	Stainless steel	25%

Supplementary Datasets

Dataset S1 (separate file). Temperature data corresponding to the five most populous cities in the United States.

Dataset S2 (separate file). Sunrise time data corresponding to the five most populous cities in the United States. Highlighted cells are adjusted for daylight saving time (note that Phoenix does not observe daylight saving time).

Supplementary Material References

Chin, A.W.H., Chu, J.T.S., Perera, M.R.A., Hui, K.P.Y., Yen, H.-L., Chan, M.C.W., Peiris, M., Poon, L.L.M., 2020. Stability of SARS-CoV-2 in different environmental conditions. The Lancet Microbe 1, e10. https://doi.org/10.1016/S2666-5247(20)30003-3

Darnell, M.E.R., Taylor, D.R., 2006. Evaluation of inactivation methods for severe acute respiratory syndrome coronavirus in noncellular blood products. Transfusion 46, 1770–1777. https://doi.org/10.1111/j.1537-2995.2006.00976.x

Greatorex, J.S., Digard, P., Curran, M.D., Moynihan, R., Wensley, H., Wreghitt, T., Varsani, H., Garcia, F., Enstone, J., Nguyen-Van-Tam, J.S., 2011. Survival of influenza A(H1N1) on materials found in households: Implications for infection control. PLoS One 6, 4–9. https://doi.org/10.1371/journal.pone.0027932

Leclercq, I., Batéjat, C., Burguière, A.M., Manuguerra, J.C., 2014. Heat inactivation of the Middle East respiratory syndrome coronavirus. Influenza Other Respi. Viruses. https://doi.org/10.1111/irv.12261

McDevitt, J., Rudnick, S., First, M., Spengler, J., 2010. Role of absolute humidity in the inactivation of influenza viruses on stainless steel surfaces at elevated temperatures. Appl. Environ. Microbiol. 76, 3943–3947. https://doi.org/10.1128/AEM.02674-09

Mildrexler, D.J., Zhao, M., Running, S.W., 2006. Where are the hottest spots on Earth? Eos (Washington. DC). 87, 461–467. https://doi.org/10.1029/2006EO430002

Qin, Z., Balasubramanian, S.K., Wolkers, W.F., Pearce, J.A., Bischof, J.C., 2014. Correlated Parameter Fit of Arrhenius Model for Thermal Denaturation of Proteins and Cells. Ann. Biomed. Eng. https://doi.org/10.1007/s10439-014-1100-y

van Doremalen, N., Bushmaker, T., Morris, D.H., Holbrook, M.G., Gamble, A., Williamson, B.N., Tamin, A., Harcourt, J.L., Thornburg, N.J., Gerber, S.I., Lloyd-Smith, J.O., de Wit, E., Munster, V.J., 2020. Aerosol and Surface Stability of SARS-CoV-2 as Compared with SARS-CoV-1. N. Engl. J. Med. https://doi.org/10.1056/NEJMc2004973

van Doremalen, N., Bushmaker, T., Munster, V.J., 2013. Stability of middle east respiratory syndrome coronavirus (MERS-CoV) under different environmental conditions. Eurosurveillance 18, 1–4. https://doi.org/10.2807/1560-7917.ES2013.18.38.20590

Wright, N.T., 2003. On a Relationship Between the Arrhenius Parameters from Thermal Damage Studies. J. Biomech. Eng. 125, 300–304. https://doi.org/10.1115/1.1553974

Yap, T.F., Liu, Z., Shveda, R.A., Preston, D.J., 2020. A predictive model of the temperature-dependent inactivation of coronaviruses. Appl. Phys. Lett. 117. https://doi.org/10.1063/5.0020782